Geophysical Research Letters

RESEARCH LETTER
10.1029/2019GL083104

Dynamical Control of the Tibetan Plateau on the East Asian Summer Monsoon

Jun-Hyeok Son[1], Kyong-Hwan Seo[1,2], and Bin Wang[3]

[1]Department of Atmospheric Sciences, Division of Earth Environmental System, Pusan National University, Busan, South Korea, [2]Research Center for Climate Science, Pusan National University, Busan, South Korea, [3]Department of Atmospheric Sciences, IPRC, University of Hawaii, Honolulu, HI, USA

Key Points:
- The origin of the East Asian summer monsoon is the fluid dynamical effect due to the Tibetan Plateau
- This dynamical response to Tibetan Plateau forcing explains ~65% of total precipitation over East Asian summer monsoon region
- Mountain forced stationary Rossby waves induce zonal pressure gradient and southerly winds over East Asia

Correspondence to:
K.-H. Seo,
khseo@pusan.ac.kr

Citation:
Son, J.-H., Seo, K.-H., & Wang, B. (2019). Dynamical control of the Tibetan Plateau on the East Asian summer monsoon. *Geophysical Research Letters*, *46*, 7672–7679. https://doi.org/10.1029/2019GL083104

Received 3 APR 2019
Accepted 19 JUN 2019
Accepted article online 24 JUN 2019
Published online 8 JUL 2019

Abstract The origin of the East Asian summer monsoon (EASM)—the sole monsoon existing in the subtropics-midlatitude in the northern hemisphere—has long been recognized as an elevated heating and mechanical forcing of the Tibetan Plateau, and the land-sea zonal heat contrast. However, the relative contribution of individual processes to the generation of the East Asian summer monsoon and therefore the underlying basic physics are unexplored. Here we show that the EASM is mainly driven by the dynamical effect of the Tibetan Plateau, in which forced topographic Rossby waves induce downstream southerlies, a crucial factor in EASM precipitation. From idealized general circulation model simulations, the dynamical effect of mountains is revealed to account for ~65% of the total East Asian summer precipitation, whereas the elevated heating and land-sea heat contrast are only responsible for ~15% each and the mountain-drag effect accounts for less than 5%.

1. Introduction

The East Asian summer monsoon (EASM) has long been viewed as a response to the elevated heating and mechanical effects of the Tibetan Plateau, as well as the land-sea zonal heat contrast (Figure 1; Abe et al., 2003; Chen & Bordoni, 2014; Chiang et al., 2015, 2017; Chou et al., 2001; Kitoh, 2004; Molnar et al., 2010; Wu et al., 2007). During the northern hemisphere summer, heating over the Tibetan Plateau and Eurasian continent is known to create a thermal cyclone that forces southerly winds to the east (Chen & Bordoni, 2014; Wu et al., 2007). This thermodynamic process of inducing southerly winds through a zonal pressure gradient force between low pressure on land and high pressure over the ocean is generally explained by the response of the land-sea heat contrast, which is considered the basic mechanism of monsoon generation (Figure 2; Halley, 1686; Wu et al., 2012). The elevated heating due to the Tibetan Plateau contributes to the inward and upward advection of air parcel along the flank of the plateau. The air pumping over the Tibetan Plateau is known to enhance the large-scale cyclonic circulation around the mountain (Kitoh, 2004; Liu et al., 2007).

The mechanical effect of the Tibetan Plateau includes a flow uplift, a flow deflection, and a mountain-drag effect (Figure 1). The upward propagating gravity wave tends to decelerate flow when the wave breaks, and thus, the mountain gravity wave drag builds a characteristic meridional dipole structure with a cyclonic circulation to the south and an anticyclonic circulation to the north of the mountain (Cohen & Boos, 2017). Topographic drag is generated by the mountain-induced boundary layer turbulence (Lott & Miller, 1997). These gravity wave drag and topographic drag effects can be regarded as the mountain-drag effect. The drag effect plays a minor role in generating or enhancing the EASM (Baldwin & Vecchi, 2016; Cohen & Boos, 2017; Wu et al., 2007), which is confirmed in this study as well. On the other hand, the uplifting effect involves the generation of flows over the mountain and this leads to the formation of the stationary Rossby waves due to potential vorticity conservation (Held, 1983; Rodwell & Hoskins, 2001; Seo et al., 2015). The deflection effect splits the westerly winds impinging on the plateau to both the northern and southern slopes of the plateau, later to reconverge downstream (Kitoh, 2004; Wu et al., 2007). The cold air coming from the north and the warm moisture air blowing from the south can intensify air mass confrontation and the quasi-stationary frontal rainband (Seo et al., 2015; Tomita et al., 2011). The uplift and deflection effects are referred to as the dynamical effect.

In this study, we stress not the above-mentioned thermodynamic and mountain-drag processes but rather the dynamical effect of the Tibetan Plateau (Cohen & Boos, 2017; Held, 1983), which is related to

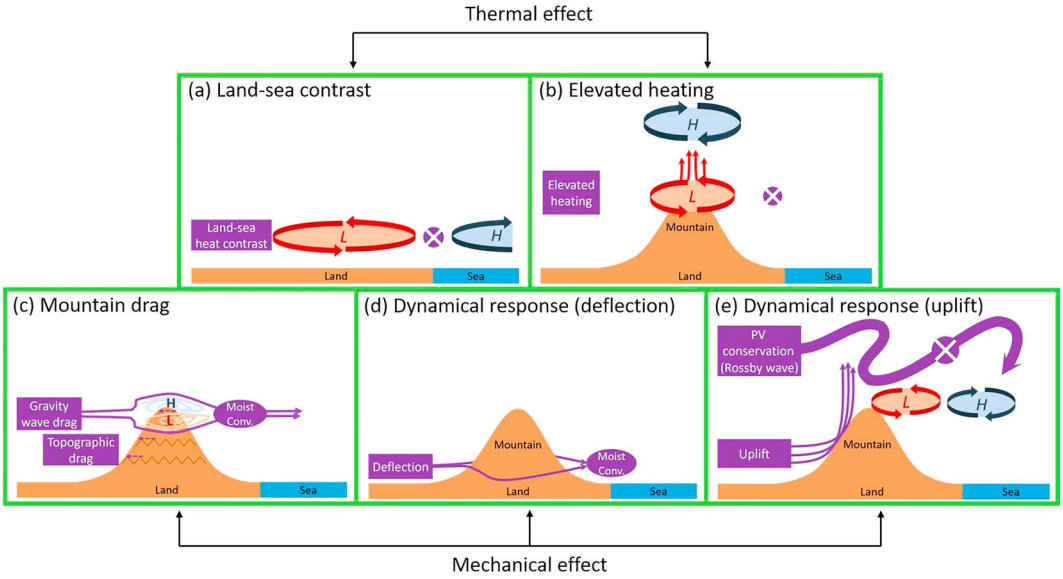

Figure 1. Schematic of various proposed factors for the formation of the East Asian summer monsoon.

topographically forced Rossby waves. The northern hemisphere stationary waves forced by the zonal flow over huge mountains, such as the Tibetan Plateau and the Rockies, cause an anticyclone over the western part of the mountain peak, a cyclone to the east, and an anticyclone further to the east. The last two stationary wave components lie over East Asia, which is similar to the zonal phase of eddies induced by the Eurasian Continent-Pacific Ocean thermal contrast (Figures 1a and 1e). However, summer amplitudes of the topographic wave are weaker than those of the winter counterpart because of the reduced strength of the subtropical jet stream. As a result, limited attention has been given to the pure dynamical impact of the Tibetan Plateau in explaining the mechanism of EASM generation.

2. Data Sets and Methods

The Global Precipitation Climatology Project (GPCP; Huffman et al., 2001) daily precipitation, the National Oceanic and Atmospheric Administration Optimum Interpolation sea surface temperature (SST) V2 (Reynolds et al., 2002), and the European Centre for Medium-Range Weather Forecasts (ECMWF) Interim Reanalysis (ERA-Interim; Dee et al., 2011) products are used. The climatological average for all atmospheric variables is calculated from 1979 to 2015, except for precipitation (1997–2015) and SST (1982–2015).

The idealized general circulation model (GCM) is based on the Geophysical Fluid Dynamics Laboratory (GFDL) Atmosphere Model, version 2.1 (AM2.1; Anderson et al., 2004). AM2.1 uses a finite-volume dynamical core (Lin, 2004), spanning 2.5° × 2.0° in the horizontal and 24 vertical levels. The models are run for 12 years, and the last 10 years are considered. All model results are displayed as ensemble averages of five individual simulations. In simulations (AMIP-type), the zonally uniform climatological SSTs varying with month are used for the oceanic boundary condition. Over land, the surface energy and water balance are conserved by the land model version 2 calculation of the surface flux, radiation exchange, and runoff.

We performed the aqua planet experiment as our simplest backbone simulation and assumed an idealized land and mountain to reflect a simplified version of reality. An idealized square of land is placed at 20–120°E and 15–70°N, where the land surface is flat at sea level and uniformly covered with grass over ground types of coarse, medium, and fine mix. To examine the effect of the Tibetan Plateau on the EASM, a Gaussian bell-shaped mountain is placed at 80–100°E and 25–45°N, with a maximum height of 5 km. For sensitivity tests, the surface albedo was raised to 0.6 at altitudes greater than 2.5 km to remove mountain elevated heating. The original albedo on the grass with no snow cover is set to be 0.18.

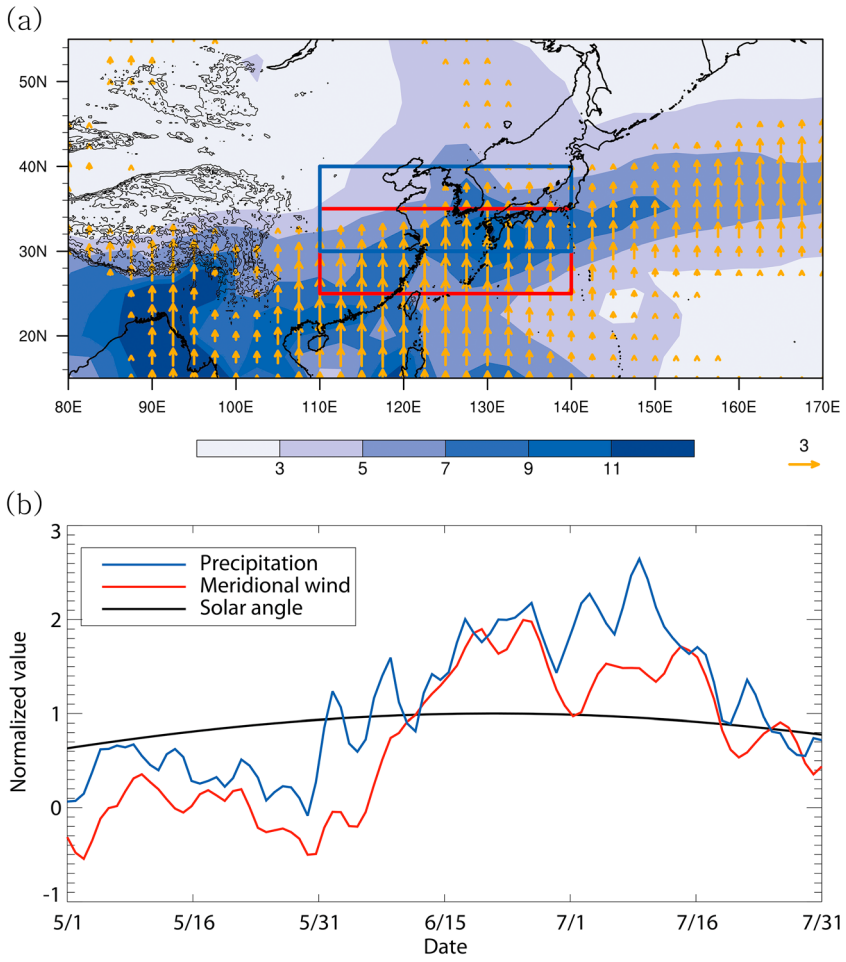

Figure 2. Climatological characteristics of East Asian summer monsoon (EASM) precipitation and meridional wind. (a) East Asian precipitation (mm/day) and southerly wind (m/s) at 600–500 hPa averaged from May to July. The EASM precipitation index is averaged over the blue box [110–140°E, 30–40° N], and the meridional wind index is the average of the red box [110–140°E, 25–35°N]. (b) The climatologically daily averaged normalized (nondimensional values) precipitation (blue line), meridional wind (red line), and solar angle (black line) time series. The precipitation or wind is normalized by using the mean and standard deviation of each variable's annual cycle (365 days).

It is known that the diabatic heating on the Tibetan Plateau is mainly due to sensible and latent heating (Wu et al., 2007), but the effects of radiative cooling and interactions among them also significantly influence the atmosphere. Therefore, the effect of elevated heating over the Tibetan Plateau is better reflected in the air temperature (Figure 3a), since it is a final product of complex thermodynamic processes (in other words, it does not represent a specific diabatic heating process such as sensible heating; Hu & Boos, 2017). A positive air temperature anomaly shown in Figure 3a represents elevated heating over the Tibetan Plateau in the observations. In the idealized land (no mountain) GCM experiment, elevated heating does not occur in the middle troposphere (Figure 3b); however, elevated heating is simulated in the idealized land and mountain experiment (Figure 3c). To remove elevated heating in the land with mountain experiment, we set the albedo to 0.6 only at the mountain surface. As a result, the albedo = 0.6 experiment does not simulate the warm temperature anomaly over the top of the mountain (Figure 3d).

To investigate other mechanical effects of mountains, we toggled on and off the topographic drag and the gravity wave parameterization schemes (Chao, 2015; Garner, 2005; Olafsson & Bougeault, 1997). In the calculation of the mountain drag effect, realistic high-resolution (1/30°) topography needs to be used. However, the use of the smooth mountains in this study produces nearly the same results as those from the realistic topography (not shown) since basically the drag effects are considerably small compared to grid-scale dynamics (Baldwin & Vecchi, 2016).

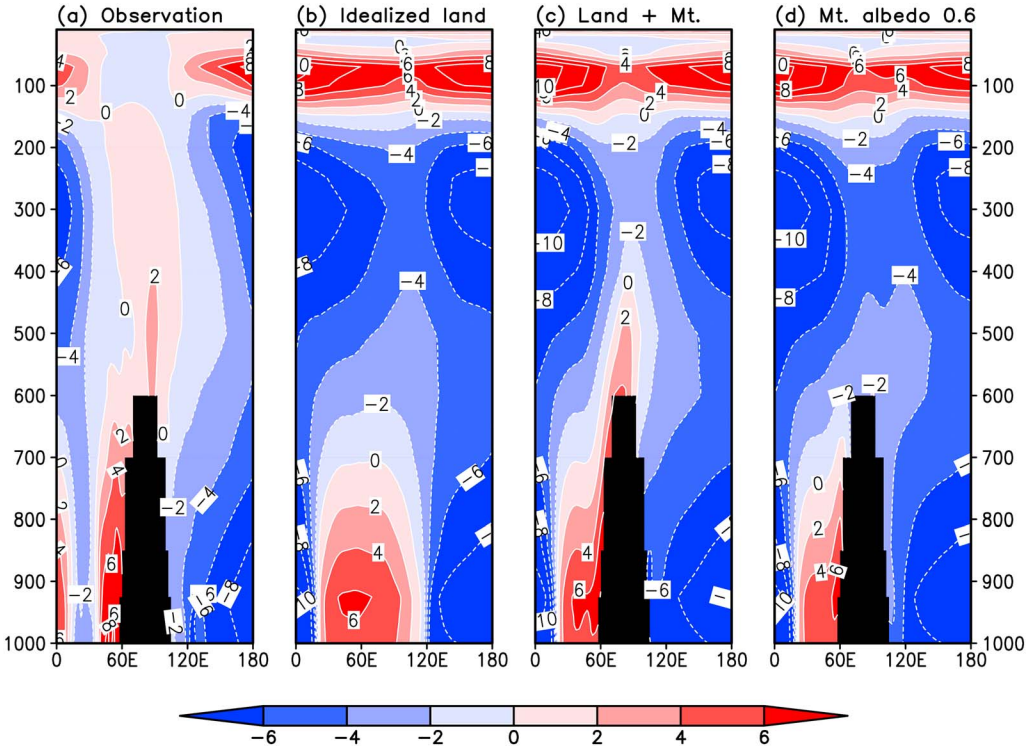

Figure 3. Tibetan heating in observations and idealized model experiments. Vertical and zonal cross section of 30°–40°N averaged air temperature anomaly (K) during June and July. (a) Air temperature anomalies in observations, and (b) general circulation model experiment of idealized land, (c) land and mountain, and (d) mountain albedo of 0.6 are calculated by deviations from the zonal average of the observations.

The experiments are very idealized, with unrealistically rectangular land, homogeneous vegetation cover, a smooth, bell-shaped mountain, and zonally uniform meridionally varying SSTs. While these experiments are not as realistic as those of a more complex, realistic GCM, they make it possible to isolate the fundamental mechanisms controlling the EASM (Chou, 2003; Voigt et al., 2016).

3. Simulation Results

The southerly winds blowing into East Asia act to supply water vapor to the EASM front (Chou et al., 2009; Figure 2a). The correlation between the meridional wind and precipitation is estimated to be as high as 0.84 from May to July (Figure 2b), indicating their strong physical connection. The summer evolution of the meridional wind and precipitation is distinct from that of the solar angle (Figure 2b). Here a question arises as to which of the following factors plays the dominant role in the development of the barotropic monsoonal southerly wind—the elevated heating over the Tibetan Plateau, mechanical (i.e., dynamical and mountain-drag) effects, or the land-sea heat contrast. To examine the overriding mechanism of the EASM, we designed a suite of sensitivity tests using an idealized GCM (Figure 4). See section 2 for details of the model.

The first experiment is the simplistic aqua planet simulation. The result shows a zonally elongated precipitation pattern in the typical tropical convergence zone, but the simulation does not capture the monsoon-like precipitation (Figure 4a). The second experiment is an idealized land simulation, where significant precipitation forms in the southeastern portion of the land, consistent with observational evidence of the South Asian monsoon precipitation. However, precipitation does not appear in the EASM domain (Figure 4b). An idealized land with mountain simulation is the third experiment, which contains the effects of elevated heating, land-sea heat contrast, dynamical forcing, and mountain drag, all resulting in contributions to the EASM precipitation (Figure 4c). For the fourth simulation, to eliminate the elevated heat effect over the

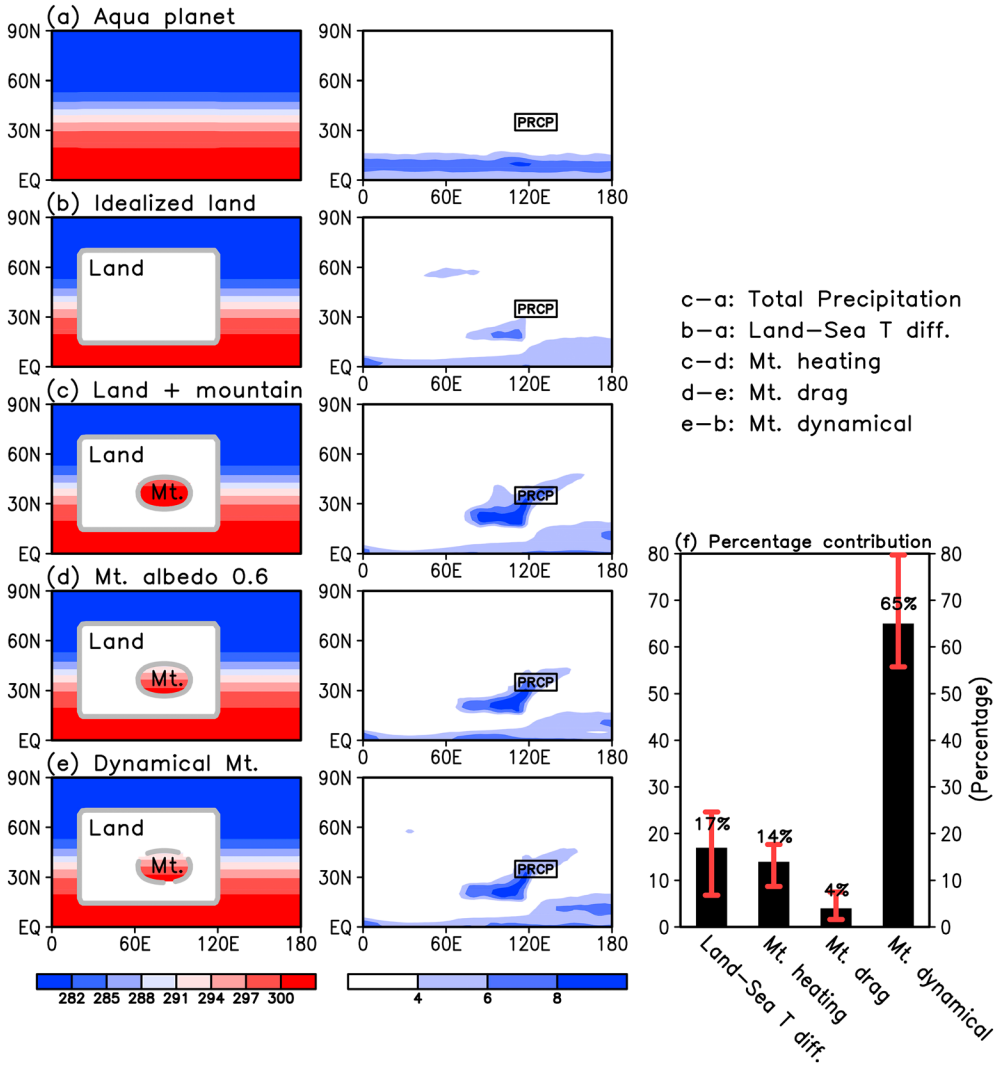

Figure 4. Idealized model experiments for East Asian summer monsoon (EASM) precipitation. The general circulation model simulations of (a) aqua planet, (b) idealized land, (c) idealized land with mountain, (d) mountain albedo of 0.6, and (e) pure dynamical mountain. The left panel denotes the model settings, illustrating the land-sea distribution and mountain characteristics (K), and the middle panel shows corresponding precipitation (mm/day) during June and July. The PRCP box refers to the domain of observed peak EASM rainfall (same as Figure 2a). (f) The percentage contributions of dynamical, land-sea thermal difference, mountain heating, and mountain-drag effects on the EASM precipitation. The error bar shows the spread of the five ensemble member simulations.

mountain, the surface albedo is raised to 0.6 from a normal grass-type albedo of 0.18, set at altitudes greater than 2.5 km (Boos & Kuang, 2013) (Figure 4d). The surface absorbing the solar radiation emits long-wave radiation and sensible and latent heat fluxes to the atmosphere, warming the atmosphere. Increasing the surface albedo leads to reduction or elimination of the elevated heating by decreasing the surface heat source. This simulation result demonstrates that EASM precipitation occurs regardless of the presence or absence of elevated heating over the mountain (Figures 3, 4c, and 4d). In the fifth simulation, the mountain drag effect was removed from the fourth simulation by turning off both the topographic drag and mountain gravity wave drag parameterization schemes. Consequently, the mountain-forced dynamical and land-sea zonal heat contrast effects were included in this simulation. It is remarkable to see that pure dynamical forcing of the mountain is enough to simulate the EASM rainband (Figures 4e and 4f). Both thermodynamic and mountain-drag forcings have small effects.

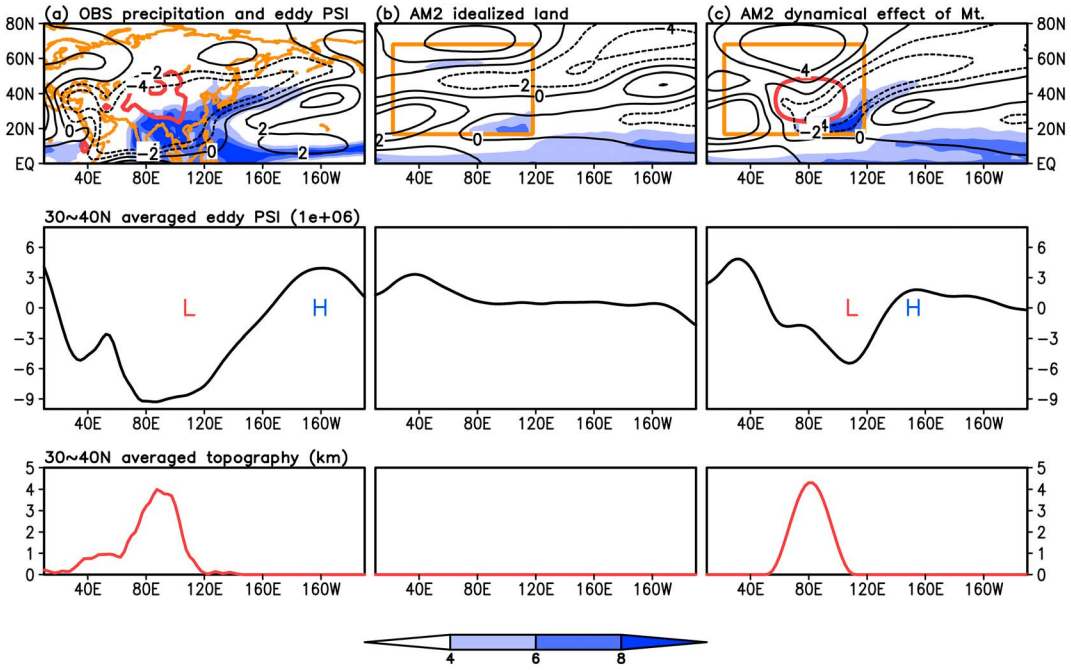

Figure 5. Observations and dynamical model simulations of the Asian summer monsoon. (a) Observations, (b) general circulation model simulation on idealized land, and (c) result of idealized land and dynamical mountain (excluding elevated heating and drag effects). The horizontal distribution of the eddy streamfunction (m^2/s, black lines) at 600–500 hPa and precipitation (blue shading) are illustrated on the top panel from June to July. The middle and bottom panels are 30–40°N averaged eddy streamfunction (black line) and topography (red line), respectively.

The elevated heating of the Tibetan Plateau has been considered the dominant source of EASM generation; however, according to our GCM simulation results, the dynamical effect is the major contributor of the EASM. Since the third experiment is a total simulation, the quantitative contribution of the land-sea thermal contrast, elevated heating, dynamical forcing, and mountain-drag effect for the formation of the EASM precipitation can be evaluated (Figure 4f). Subtracting the aqua planet simulation precipitation from the idealized land experiment yields the proportion of the pure land-sea thermal contrast, which is estimated to comprise only 17% of the total EASM domain-averaged precipitation. Subtracting the fourth simulation from the third provides evidence of the mountain heating effect, which accounts for 14%. The mountain-drag effect, which is estimated by subtracting the fifth simulation from the fourth, explains only 4%. On the other hand, the dynamical impact, which is obtained by subtracting the second simulation from the fifth experiment, accounts for as much as 65% of the total precipitation. The relative contributions of each component to the formation of the southerly winds are similar to those for precipitation (not shown).

In the observations, a strong pressure gradient occurs in the EASM region, and the precipitation stretches northeastward from southeastern China toward Korea and Japan (upper and middle panels of Figure 5a). Although the land-sea heat difference is thought to generate low and high pressures during summer over the Eurasian Continent and the Pacific Ocean, respectively (Chen & Bordoni, 2016; Shaw & Voigt, 2015; Wu et al., 2012), our idealized land experiment demonstrates that the zonal heat difference for the flat surface produces an extremely weak pressure gradient and therefore weak precipitation (Figure 5b). Quasi-stationary eddies, appearing in the observations and the dynamical forcing result of the mountain experiment (Figsure 5a and 5c), can be attributed to be orography-forced barotropic Rossby waves (Held, 1983; Rodwell & Hoskins, 2001). Tibetan Plateau heating added to the land-sea heat contrast effect can contribute to the zonal pressure gradient over East Asia, but the EASM southerly winds are mainly driven by the dynamical response to mountain forcing (Figures 4f and 5c). One may consider the sum of the land-sea zonal heat contrast on the flat surface (Figure 1a) and elevated surface heating (Figure 1b) as the land-sea contrast effect, which then explains ~30% of the East Asian precipitation. In contrast, the mechanical effect of mountain accounts for ~70%.

The spatial bias of the downstream anticyclone over the ocean (Figures 5a and 5c) may come from the absence of air-sea interactions in our GCM experiments (Matsumura & Horinouchi, 2016; Wang et al., 2000, 2013; Wang & Zhang, 2002; Zhou et al., 2009). Model results using realistic topography (not shown) show nearly identical dynamical responses of the Tibetan Plateau to those from the above idealized GCM experiments.

4. Discussion and Conclusion

From idealized GCM experiments and observations, the dynamical impact of the Tibetan Plateau was determined to be the predominant mechanism for EASM origin. The zonal pressure gradient formed by topographically induced Rossby waves and the subsequent moisture transport from the south are the most crucial process in sustaining the EASM rainband. Moreover, as an implication of this conclusion, this physical mechanism can be applied to any mountain area, such as the Rockies, Andes, or the Ural Mountains (Chen et al., 2001; Vera et al., 2006). However, the detailed weather and climate responses are unequal to those of the EASM due to such characteristics as different land-sea configurations, locations of mountain peaks, and the properties of the boundary. This study only deals with the origin of the climatological EASM, but for estimation of predictability, its interannual or interdecadal variation is more relevant, which will be investigated in the future. Recent work suggests that the seasonal transitions of the EASM are controlled by the meridional position of the midlatitude westerly jet with respect to the location of the Tibetan Plateau (Chiang et al., 2015, 2017). However, its underlying mechanism is still unclear. For the physical mechanism that is responsible for the EASM formation, we will present in the future how forced topographic Rossby wave makes the downstream southerlies and how the amplitude of the downstream stationary Rossby wave is dependent upon the upstream westerly wind impinging on the Tibetan Plateau.

Acknowledgments
This work was supported by the National Research Foundation of Korea (NRF) grant funded by the Korea government (MSIP; NRF-2018R1A2A2A05018426) and the KMA Research and Development Program under grant KMI2018-01012. We would like to thank Daehyun Kim for the discussion of Rossby wave dynamics, Stephen Garner and Jin-Ho Yoon for their helpful comments, and the Editor Suzanna Camargo for the thoughtful comments and encouragement. We are grateful to the two reviewers for their valuable comments and suggestions, which improved the paper. The ERA-Interim reanalysis is available at http://www.ecmwf.int, precipitation is at https://precip.gsfc.nasa.gov, SST is downloaded from https://www.esrl.noaa.gov/psd/data/gridded/data.noaa.oisst.v2.html, and the AM2.1 idealized model simulation products are stored at https://climate.pusan.ac.kr/climate1/48095/subview.do.

References

Abe, M., Kitoh, A., & Yasunari, T. (2003). An evolution of the Asian summer monsoon associated with mountain uplift—Simulation with the MRI atmosphere–ocean coupled GCM. *Journal of the Meteorological Society of Japan*, *81*(5), 909–933. https://doi.org/10.2151/jmsj.81.909

Anderson, J., Balaji, V., Broccoli, A. J., Cooke, W. F., Delworth, T. L., Dixon, K. W., et al. (2004). The new GFDL global atmosphere and land model AM2–LM2: Evaluation with prescribed SST simulations. *Journal of Climate*, *17*(24), 4641–4673. https://doi.org/10.1175/jcli-3223.1

Baldwin, J., & Vecchi, G. (2016). Influence of the Tian Shan on arid extratropical Asia. *Journal of Climate*, *29*(16), 5741–5762. https://doi.org/10.1175/JCLI-D-15-0490.1

Boos, W., & Kuang, Z. (2013). Sensitivity of the South Asian monsoon to elevated and non-elevated heating. *Scientific Reports*, *3*(1), 1192. https://doi.org/10.1038/srep01192

Chao, W. (2015). Correction of excessive precipitation over steep and high mountains in a GCM: A simple method of parameterizing the thermal effects of subgrid topographic variation. *Journal of the Atmospheric Sciences*, *72*(6), 2366–2378. https://doi.org/10.1175/JAS-D-14-0336.1

Chen, J., & Bordoni, S. (2014). Orographic effects of the Tibetan Plateau on the East Asian Summer monsoon: An energetic perspective. *Journal of Climate*, *27*(8), 3052–3072. https://doi.org/10.1175/JCLI-D-13-00479.1

Chen, J., & Bordoni, S. (2016). Early summer response of the East Asian summer monsoon to atmospheric CO_2 forcing and subsequent sea surface warming. *Journal of Climate*, *29*(15), 5431–5446. https://doi.org/10.1175/JCLI-D-15-0649.1

Chen, P., Hoerling, M. P., & Dole, R. M. (2001). The origin of the subtropical anticyclones. *Journal of the Atmospheric Sciences*, *58*(13), 1827–1835. https://doi.org/10.1175/1520-0469(2001)058<1827:TOOTSA>2.0.CO;2

Chiang, J. C. H., Fung, I. Y., Wu, C. H., Cai, Y., Edman, J. P., Liu, Y., et al. (2015). Role of seasonal transitions and westerly jets in East Asian paleoclimate. *Quaternary Science Reviews*, *108*, 111–129. https://doi.org/10.1016/j.quascirev.2014.11.009

Chiang, J. C. H., Swenson, L. M., & Kong, W. (2017). Role of seasonal transitions and the westerlies in the interannual variability of the East Asian summer monsoon precipitation. *Geophysical Research Letters*, *44*, 3788–3795. https://doi.org/10.1002/2017GL072739

Chou, C. (2003). Land–sea heating contrast in an idealized Asian summer monsoon. *Climate Dynamics*, *21*(1), 11–25. https://doi.org/10.1007/s00382-003-0315-7

Chou, C., Huang, L.-F., Tseng, L., Tu, J.-Y., & Tan, P.-H. (2009). Annual cycle of rainfall in the western North Pacific and East Asian sector. *Journal of Climate*, *22*(8), 2073–2094. https://doi.org/10.1175/2008JCLI2538.1

Chou, C., Neelin, J. D., & Su, H. (2001). Ocean–atmosphere–land feedbacks in an idealized monsoon. *Quarterly Journal of the Royal Meteorological Society*, *127*(576), 1869–1891. https://doi.org/10.1002/qj.49712757602

Cohen, N. Y., & Boos, W. R. (2017). The influence of orographic Rossby and gravity waves on rainfall. *Quarterly Journal of the Royal Meteorological Society*, *143*(703), 845–851. https://doi.org/10.1002/qj.2969

Dee, D., Uppala, S. M., Simmons, A. J., Berrisford, P., Poli, P., Kobayashi, S., et al. (2011). The ERA-Interim reanalysis: Configuration and performance of the data assimilation system. *Quarterly Journal of the Royal Meteorological Society*, *137*(656), 553–597. https://doi.org/10.1002/qj.828

Garner, S. T. (2005). A topographic drag closure built on an analytical base flux. *Journal of the Atmospheric Sciences*, *62*(7), 2302–2315. https://doi.org/10.1175/JAS3496.1

Halley, E. (1686). An historical account of the trade winds, and monsoons, observable in the seas between and near the tropics, with an attempt to assign the physical cause of said winds. *Philosophical Transactions of the Royal Society*, *16*, 153–168.

Held, I. M. (1983). Stationary and quasi-stationary eddies in the extratropical troposphere. Theory. In B. J. Hoskins & R. P. Pearce (Eds.), *Large-Scale Dynamical Processes in the Atmosphere* (pp. 127–168). London: Academic Press.

Hu, S., & Boos, W. R. (2017). The physics of orographic elevated heating in radiative–convective equilibrium. *Journal of the Atmospheric Sciences*, *74*(9), 2949–2965. https://doi.org/10.1175/JAS-D-16-0312.1

Huffman, G. J., Adler, R. F., Morrissey, M. M., Curtis, S., Joyce, R., McGavock, B., & Susskind, J. (2001). Global precipitation at one-degree daily resolution from multi-satellite observations. *Journal of Hydrometeorology*, *2*(1), 36–50. https://doi.org/10.1175/1525-7541(2001)002<0036:gpaodd>2.0.co;2

Kitoh, A. (2004). Effects of mountain uplift on East Asian summer climate investigated by a coupled atmosphere–ocean GCM. *Journal of Climate*, *17*(4), 783–802. https://doi.org/10.1175/1520-0442(2004)017<0783:EOMUOE>2.0.CO;2

Lin, S.-J. (2004). A "vertically Lagrangian" finite-volume dynamical core for global models. *Monthly Weather Review*, *132*(10), 2293–2307. https://doi.org/10.1175/1520-0493(2004)132<2293:AVLFDC>2.0.CO;2

Liu, Y., Hoskins, B., & Blackburn, M. (2007). Impact of Tibetan orography and heating on the summer flow over Asia. *Journal of the Meteorological Society of Japan*, *85B*, 1–19. https://doi.org/10.2151/jmsj.85B.1

Lott, F., & Miller, M. J. (1997). A new subgrid-scale orographic drag parametrization: Its formulation and testing. *Quarterly Journal of the Royal Meteorological Society*, *123*(537), 101–127. https://doi.org/10.1002/qj.49712353704

Matsumura, S., & Horinouchi, T. (2016). Pacific Ocean decadal forcing of long-term changes in the western Pacific subtropical high. *Scientific Reports*, *6*(1), 37765. https://doi.org/10.1038/srep37765

Molnar, P., Boos, W. R., & Battisti, D. S. (2010). Orographic controls on climate and paleoclimate of Asia: Thermal and mechanical roles for the Tibetan Plateau. *Annual Review of Earth and Planetary Sciences*, *38*(1), 77–102. https://doi.org/10.1146/annurev-earth-040809-152456

Olafsson, H., & Bougeault, P. (1997). The effect of rotation and surface friction on orographic drag. *Journal of the Atmospheric Sciences*, *54*(1), 193–210. https://doi.org/10.1175/1520-0469(1997)054<0193:TEORAS>2.0.CO;2

Reynolds, R. W., Rayner, N. A., Smith, T. M., Stokes, D. C., & Wang, W. (2002). An improved in situ and satellite SST analysis for climate. *Journal of Climate*, *15*(13), 1609–1625. https://doi.org/10.1175/1520-0442(2002)015<1609:AIISAS>2.0.CO;2

Rodwell, M. J., & Hoskins, B. J. (2001). Subtropical anticyclones and summer monsoons. *Journal of Climate*, *14*(15), 3192–3211. https://doi.org/10.1175/1520-0442(2001)014<3192:SAASM>2.0.CO;2

Seo, K.-H., Son, J.-H., Lee, J.-Y., & Park, H.-S. (2015). Northern East Asian monsoon precipitation revealed by air mass variability and its prediction. *Journal of Climate*, *28*, 6221–6233. https://doi.org/10.1175/JCLI-D-14-00526.1

Shaw, T., & Voigt, A. (2015). Tug of war on summertime circulation between radiative forcing and sea surface warming. *Nature Geoscience*, *8*, 560–566. https://doi.org/10.1038/ngeo2449

Tomita, T., Yamaura, T., & Hashimoto, T. (2011). Interannual variability of the baiu season near Japan evaluated from the equivalent potential temperature. *Journal of the Meteorological Society of Japan*, *89*(5), 517–537. https://doi.org/10.2151/jmsj.2011-507

Vera, C., Higgins, W., Amador, J., Ambrizzi, T., Garreaud, R., Gochis, D., et al. (2006). Toward a unified view of the American monsoon systems. *Journal of Climate*, *19*(20), 4977–5000. https://doi.org/10.1175/JCLI3896.1

Voigt, A., Biasutti, M., Scheff, J., Bader, J., Bordoni, S., Codron, F., et al. (2016). The tropical rain belts with an annual cycle and continent model intercomparison project: TRACMIP. *Journal of Advances in Modeling Earth Systems*, *8*, 1868–1891. https://doi.org/10.1002/2016MS000748

Wang, B., Wu, R., & Fu, X. (2000). Pacific-East Asia teleconnection: How does ENSO affect East Asian climate? *Journal of Climate*, *13*(9), 1517–1536. https://doi.org/10.1175/1520-0442(2000)013<1517:PEATHD>2.0.CO;2

Wang, B., Xiang, B., & Lee, J.-Y. (2013). Subtropical High predictability establishes a promising way for monsoon and tropical storm predictions. *Proceedings of the National Academy of Sciences of the United States of America*, *110*(7), 2635–2640. https://doi.org/10.1073/pnas.1212646110

Wang, B., & Zhang, Q. (2002). Pacific-East Asian teleconnection. Part II: How the Philippine Sea anomalous anticyclone is established during El Nino development. *Journal of Climate*, *15*(22), 3252–3265. https://doi.org/10.1175/1520-0442(2002)015<3252:PEATPI>2.0.CO;2

Wu, G. X., Liu, Y., He, B., Bao, Q., Duan, A., & Jin, F.-F. (2012). Thermal controls on the Asian summer monsoon. *Scientific Reports*, *2*(1), 404. https://doi.org/10.1038/srep00404

Wu, G. X., Liu, Y., Zhang, Q., Duan, A., Wang, T., Wan, R., et al. (2007). The influence of the mechanical and thermal forcing of the Tibetan Plateau on the Asian climate. *Journal of Hydrometeorology*, *8*(4), 770–789. https://doi.org/10.1175/JHM609.1

Zhou, T. J., Yu, R., Zhang, J., Drange, H., Cassou, C., Deser, C., et al. (2009). Why the western Pacific subtropical high has extended westward since the late 1970s. *Journal of Climate*, *22*(8), 2199–2215. https://doi.org/10.1175/2008JCLI2527.1